The EuroBiotech Journal
RESEARCH ARTICLE
Pharmaceutical Biotechnology

Synthesis, Characterization, and Optimization of Green Silver Nanoparticles Using *Neopestalotiopsis clavispora* and Evaluation of Its Antibacterial, Antibiofilm, and Genotoxic Effects

Tuğba Kahraman[1], Safiye Elif Korcan[2], Recep Liman[1], İbrahim Hakkı Ciğerci [3], Yaser Acikbas[4], Muhsin Konuk[5,*], Gülderen Uysal Akkuş[6]

Abstract

Silver nanoparticles (AgNPs) have been used in a variety of biomedical applications in the last two decades, including antimicrobial, anti-inflammatory, and anticancer treatments. The present study highlights the extracellular synthesis of silver nanoparticles AgNPs using *Neopestalotiopsis clavispora* MH244410.1 and its antibacterial, antibiofilm, and genotoxic properties. Locally isolated *N. clavispora* MH244410.1 was identified by Internal transcribed spacer (ITS) sequences of nuclear ribosomal DNA. Optimization of synthesized AgNPs was performed by using various parameters (pH (2, 4, 7, 9 and 12), temperature (25, 35 and 45 °C), and substrate concentration (0.05, 0.1, 0.15, 0.2 and 0.25 mM)). After 72 hours of incubation in dark conditions, the best condition for the biosynthesis of AgNPs was determined as 0.25 mM metal concentration at pH 12 and 35 °C. Fungal synthesized AgNPs were characterized via spectroscopic and microscopic techniques such as Fouirer Transform Infrared Spectrophotometer (FTIR), UV-Visible Spectroscopy, and Transmission Electron Microscopy (TEM). The average size of the AgNPs was determined less than 60 nm using the TEM and Zetasizer measurement system (measured in purity water suspension). The characteristic peak of AgNPs was observed at ~414 nm from UV-Vis results. Antibacterial and genotoxic activity of synthesized AgNPs (0.1, 1, and 10 ppm) were also determined by using the agar well diffusion method and *in vivo* Somatic Mutation and Recombination Test (SMART) in *Drosophila melanogaster*. AgNPs exhibited potential antimicrobial activity against all the tested bacteria (*Bacillus subtilis*, *Staphylococcus aureus*, and *Pseudomonas aeruginosa*) except *Escherichia coli* in a dose-dependent manner. AgNPs did not induce genotoxicity in the *Drosophila* SMART assay. 79.33, 65.47, and 41.95% inhibition of biofilms formed by *P. aeruginosa* were observed at 10, 1, and 0.1 ppm of AgNPs, respectively. The overall results indicate that *N. clavispora* MH244410.1 is a good candidate for novel applications in biomedical research.

Keywords: FTIR, *Neopestalotiopsis clavispora*, UV-vis spectroscopy, SMART, TEM

[1] Molecular Biology and Genetics Department, Faculty of Arts and Sciences, Uşak University, 1 Eylül Campus, 64300, Uşak, Turkey
[2] Health Services Vocational School Medical Laboratory Program. Uşak University1 Eylül Campus, 64300, Uşak, Turkey
[3] Molecular Biology and Genetics Department, Faculty of Science and Literatures, Afyon Kocatepe University, 03200, Afyon, Turkey
[4] Department of Materials Science and Nanotechnology Engineering, Faculty of Engineering, Usak University, Usak, 64200, Turkey
[5] Biotechnology Research and Application Center, University of Üsküdar, 34600-Istanbul, Turkey.
[6] Chemistry Department, Faculty of Science and Literatures, Afyon Kocatepe University, 03200, Afyon, Turkey
Corresponding author:
Prof Muhsin KONUK, PhD
Üsküdar University, School of Engineering and Natural Sciences, Molecular Biology and Genetics Department, 34662-Istanbul-Turkey
E-mail: mkonuk@gmail.com

DOI: 10.2478/ebtj-2021-0020

Introduction

The reduction of silver ions by a variety of chemical or biological agents can yield AgNPs. The biological methods which involve nanoparticle synthesis have exhibited higher effectiveness than that of chemical methods on account of slower kinetics; this provides a greater degree of control over crystal growth and a reduction in capital expenses. Such biogenic synthesis methods are easy, safe, renewable, and economical, offering greater biocompatibility through the use of nanoparticles. In particular, fungal AgNPs synthesis is environmentally safe on account of the elimination of dangerous compounds such as hydrazine supports (1,2); such synthesis also does not require elevated temperatures and prolonged synthesis periods. These particles have also been confirmed to be three times more stable than those produced in non-biological methods (3). In addition, fungal biomass can be easily obtained and no additional steps are required for extracting the filtrate. Due to the aforementioned greater stability, fungal biomass can be utilized in the large-scale synthesis of nanoparticles using simple purification methods including filtration, dialysis, and ultracentrifugation due to their higher resistance to agitation and pressure. Furthermore, optimization of the nanoparticles can be achieved by adjusting pH, tem-

perature, agitation, light, amount of biomass and culture medium, etc. (6-10).

The synthesis of fungal AgNPs which is mediated extracellularly or intracellularly has been used in many industrial and medicinal applications due to efficient antimicrobial, antifungal, antioxidant immunomodulating, and anticancer activities (11-15) and further on account of their high tolerance of metals and ability to produce large amounts of extracellular protein, which contributes to nanoparticle stability.

The genus Pestalotiopsis contains a wide range of secondary metabolites with several properties; including antitumor, antifungal, and antimicrobial (16-18). The discovery of metal-tolerant endophytic fungi for the synthesis of metal nanoparticles could be of further major advantage (19-21). *N. clavispora*, a species linked to the Pestalotiopsis genus, has been used as an effective biosorbent for the removal of Cd(II) and Zn (II) from an aqueous solution (22).

In this study, we report the synthesis of AgNPs using cell-free filtrate (CFF) of *N. clavispora* for the first time, with the stock locally isolated from decaying wood samples. Characterization of synthesized AgNPs was performed by using UV-Vis spectroscopy, FTIR, SEM, and TEM equipment. Optimization of extracellular fungal AgNPs biosynthesis was pursued via various parameters including pH, temperature, substrate concentration, and reaction time. The antibacterial, antibiofilm, and genotoxic properties of the synthesized AgNPs were evaluated.

Materials and Methods

Isolation and identification of *N. clavispora*

The fungal strain used for the biosynthesis of AgNPs was isolated from decaying wood samples in Usak University Campus, Turkey (38° 40′ 08″ N and 29° 19′ 44″ E). 1 g of grounded wood sample was mixed with 10 mL of sterile distilled water and then shaking in an incubator at 110 rpm for 15 min at 27±2 °C. 0.1 mL mixture was incubated onto Potato Dextrose Agar (PDA, Merck 110130) for 7 days at 28±2 °C in the dark. After this, the sample was sub-cultured to achieve a pure culture on PDA and kept at 4 °C to use for future studies. Morphological properties of fungus were determined on Czapek-Dox Agar (CDA, Merck 105460) and Malt Extract Agar (MEA, Merck 105398) according to Biju et al. (23).

According to the manufacturer's instructions, total DNA isolation from a single colony of fungus was carried out using the EurX GeneMATRIX Plant&Fungi DNA isolation kit (Poland). 30 µL of Activation Buffer P was added to the spin column without spin and kept at room temperature for 10 min. Fungal tissue was homogenized with a cooled mortar and pestle under liquid nitrogen. 20 mg dry fungal tissue was placed in an empty Eppendorf tube; 400 µL of Lysis Buffer F, 3 µL of RNase A, and 10 µL of Protein kinase K were added. The tube was mixed and incubated at 65 °C for 30 min. After adding 130 µL Buffer AC, the tube was incubated for 5 min on ice. The sample was centrifuged for 10 min at 14000×g. The mixture (400 µL supernatant, 350 µL buffer Sol P and 250 µL 96% ethanol) was centrifuged for 1 min at 12000×g. After 600 µL of lysate was transferred to the DNA binding spin column, the sample was centrifuged for 1 min at 11000×g. Pellet was washed with 500 µL of Wash PX two times at 11000×g for 1 min. Spin columns were placed in a new tube and 50-150 µL of elution buffer was added to elute the bound DNA. Isolated DNA was stored at -20 °C. The universal primer ITS1 (5'- TCC GTA GGT GAA CCT GCG G -3') and ITS4 (5'- TCC TCC GCT TAT TGA TAT GC -3') were used to amplify to ITS sequences of nuclear ribosomal DNA) according to Gardes and Bruns (24). The amplification conditions were set as follows: initial denaturation at 95 °C for 5 min, 35 cycles at 95 °C for 45 s (denaturing), annealing temperature at 57 °C for 45 s, followed by extension at 72 °C for 60 s, and finally 72 °C for 5 min (final elongation). PCR reaction was performed with Solis Biodyne (Estonia) FIREPol® DNA Polymerase Taq polymerase enzyme. After PCR, a single band was obtained in agarose gel using 100 bp DNA Ladder Ready to Load (Solis BioDyne) marker, and it was observed that the PCR process was successful. ExoSAP-IT™ PCR Product Cleanup Reagent (ThermoFisher Scientific, USA) was used to purify PCR products. For this purpose mix 5 µL of a post-PCR reaction product with 2 µL of ExoSAPIT™ reagent for a combined 7 µL reaction volume. The ABI 3730XL Sanger sequencing device (Applied Biosystems, Foster City, CA) and the BigDye Terminator v3.1 Cycle sequencing kit were used for the Sanger sequencing. Consensus sequences were used to scan for homologous sequences using the Basic Local Alignment Search Tool (BLAST) program at the National Center for Biotechnology Data (NCBI; http://www.ncbi.nlm.nih.gov).

Biosynthesis of AgNPs using CFF

Biosynthesis of silver nanoparticles was done according to Maliszewska et al. (25) with slight modifications. Fungal isolate was grown in 100 mL flask containing medium (0.025 g/L yeast extract, 0.012 g/L $CaCl_2 2H_2O$, 0.05 g/L $MgSO_4 7H_2O$, 1 g/L $NH_4H_2PO_4$, and 10 g/L glucose) at 27 °C on a rotary shaker at 110 rpm 7 d and then filtered with Whatman filter paper No. 1 to obtain fungal biomass. The mixture (3.5 g fungal biomass and 150 mL sterile distilled water) was agitated at 27± 2°C in an orbital shaker at 125 rpm for 24 h. After filtration, CFF was mixed with 2.5 mM $AgNO_3$ in a ratio of 1:9, and then the mixture was agitated at 27± 2°C in an orbital shaker (125 rpm) for 72 h. When the color turns brown, the absorbance of fungal synthesized AgNPs was scanned in the range of 200-800 nm on a UV-vis spectrophotometer (Shimadzu, UV-1800) at 1 nm resolution. The CFF and 2.5 mM $AgNO_3$ were used as controls.

Optimization for fungal synthesized AgNPs

Optimization of extracellular fungal AgNPs biosynthesis for AgNPs formation using various parameters including pH (2, 4, 7, 9 and 12; at 25±2 °C ; substrate concentration 0.25 mM $AgNO_3$), temperature (25, 35 and 45 °C; at pH 7; substrate concentration 0.25 mM $AgNO_3$), reaction time (from 8 to72 hour; at pH 7; substrate concentration 0.25 mM $AgNO_3$) and substrate concentration (substrate concentration, 0.05, 0.1, 0.15, 0.25mM; at pH 7 and 0.25 mM $AgNO_3$;) were determined ac-

cording to Sobhy et al. (26) with minor changes until UV measurements were fixed. Each variable was optimized by varying only a single parameter.

Characterization of Silver Nanoparticles

Perkin Elmer 1605 FTIR System carried out the characterization of functional groups on the surface of the synthesized AgNPs. Spectrum BX spectrophotometer was screened in spectra of 4000-450 cm^{-1} (27). The size and shape of the synthesized AgNPs were determined by TEM (Hitachi TEM HT 7800) at 100kV voltage. Average nanoparticle sizes were determined by the amount of approximately 100 nanoparticles in various regions of the growing sample. Also, the zeta potential of silver nanoparticles was determined on the MALVERN NANO-ZS device.

The antimicrobial activity of the AgNPs

Antibacterial effects of green synthesized AgNPs, $AgNO_3$ and CFF were evaluated on, and *Bacillus subtilis*, *Staphylococcus aureus* ATCC 25923, *Pseudomonas aeruginosa* ATCC 27853, and *Escherichia coli* ATCCC 25922 using the agar well diffusion method (28). Under aseptic conditions, MHA agar plates (Merck, 1.05437) were inoculated with bacterial (0.5 McFarland) strain. Wells (R=6mm) were filled with 50 µL fungal synthesized of AgNPs (10, 1 and 0.1 ppm), CFF and 0.25 mM $AgNO_3$. After plates were incubated at 24 h for 37 °C, inhibition zones have been recorded in mm in diameters. Antibiotic sensitivity of bacteria was also determined by the disc diffusion method according to the guideline established by the CLSI were used as control groups. Both experiments have been conducted in triplicate.

Biofilm inhibition of AgNPs

Biofilm inhibition assay was performed according to Sandberg et al. (29) with minor modifications. Fresh, exponentially grown *P. aerouginosa* ATCC 27853 culture (106 CFU/mL) was used for biofilm inhibition assay. Subsequently, different concentrations of AgNPs (10, 1, and 0.1 ppm) were added (1/1 v/v) to the *P. aerouginosa* cultures and incubated at 37 °C for 24 h. Following incubation, samples were gently washed two times with sterile distilled water to remove the medium. The biofilms were stained with a 0.5% (w/v) crystal violet at 27±2 °C for 45 min. After washing 3 times with distilled water, 1.5 mL of ethanol: acetic acid (95: 5) mixture was added for 10 min. The antibiofilm activity of the AgNPs was determined at 570 nm by using the following formula.

% Inhibition = (A control – A sample /A control) × 100
A control: Absorbance value not containing AgNPs
A sample: Absorbance value with different concentrations of AgNPs

Drosophila melanogaster Somatic Mutation and Recombination Test (*SMART*)

Two *Drosophila* strains, flr3/TM3, BdS (female), and mwh/mwh (male) were used for the *Drosophila* SMART assay (30). The SMART test is focused on the lack of heterozygosity in the wing cells. Transheterozygous larvae were extracted from mating virgin flr3/TM3, BdS females, and mwh males (31). In this study, eggs from virgin flr3 females and mwh males were collected in a healthy nutrient medium for 8 h. After 72±4 h, 3 days old larvae were gathered under tap water using a sieve and transferred to vials containing 4.5 g of *Drosophila* Instant Medium and 9 mL of test chemicals (0.1, 1, and 10 ppm of $AgNO_3$ and AgNPs). Distilled water and 1 mM EMS were used as a negative and positive control, respectively. Adult individuals were obtained after the application. Then flies were kept at +4 °C in 70% ethanol until wing preparations were prepared. Wings were removed and mounted on microscope slides in Faure's solution. Prepared wing arrangements were tested with an optical microscope magnification of 40X.

Statistical Analysis

The data obtained in the SMART experiment were evaluated employing a computer program (MICROSTA) prepared for *Drosophila* wing somatic mutation and recombination tests. Original and alternative hypotheses were calculated by using the binomial conditional test. Kastenbaum and Bowman's (32) charts were used when original and alternative hypotheses were adopted or rejected.

Results

Isolation and identification of *N. clavispora*

Fungi were isolated from decaying wood samples in the Usak University Campus, Turkey (Fig. 1A). Colonies were white and cottony with edge undulates and circular growth appearance on CDA (Fig. 1B1-B2) and MEA (Fig. 1C1-C2). During the microscopic examination, sterile hyphae structures were observed, but conidia were not; identification according to its microscopic morphology could therefore not be made. The fungus was identified as *N. clavispora* MH244410.1 according to ITS sequences of nuclear ribosomal DNA (Total Base Number: 498 Similarity Score: 920 Series Match Rate: 100% Similarity Rate: 100%, Fig. 1D).

Biosynthesis of AgNPs using CFF

After the addition of 2.5 mM AgNO3 (1:9), the color of the CFF was altered from a light yellow to dark brown due to the reduction of the silver ion. This is the first indication of fungal synthesis AgNPs within 24 h. Figure 2 shows that the reaction had run for 24 h, and the detection of a specific absorption peak at 414 nm, indicating the formation of AgNPs.

Optimization for fungal AgNPs synthesis

The bands typical for AgNPs were observed in the wavelength range of 4010-419 nm under changing conditions. The peak was obtained at 414 nm in every tested condition, and accordingly, the bio-reduction of Ag ions in the CFF was monitored periodically by measuring UV-Vis spectroscopy at 414 nm. Different parameters including pH, temperature, substrate

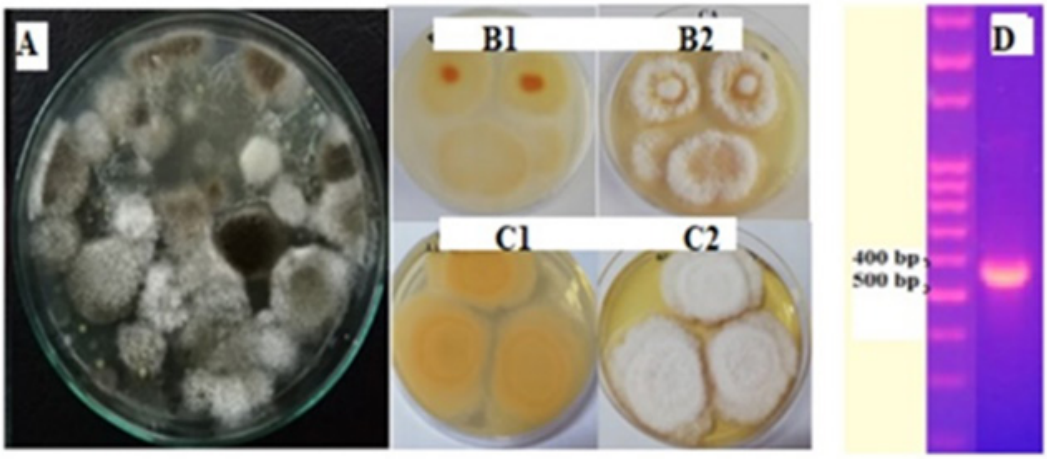

Figure 1. Isolation and identification of *N. clavispora* A: PDA was used for fungus isolation from decaying wood samples. B: Morphology of the fungus at CDA (B1: Upperside, B2: Reverse side) C: Morphology of the fungus at MEA (C1: Upperside, C2: reverse side), D; Amplification ITS profiles of *N. clavispora* at agarose gel electrophoresis.

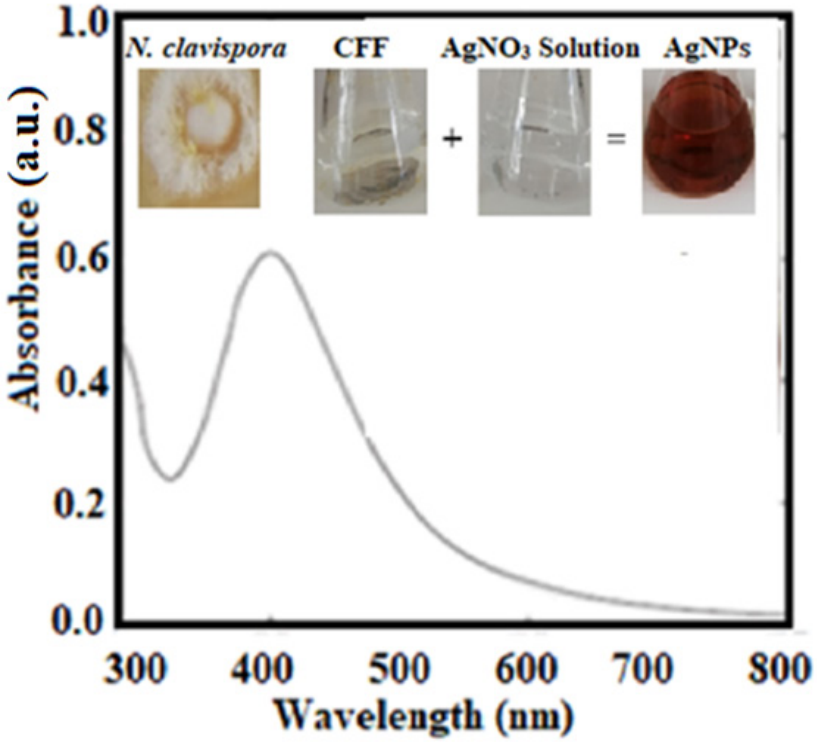

Figure 2. UV–Vis spectroscopy of AgNPs synthesized using CFF.

concentration, and reaction time are shown in Fig 3. A pH range of 2–12 was selected for this study. Absorbance is shown to increase with pH, suggesting that an alkaline environment is more suitable for AgNP biosynthesis (Figure3A). The optimal temperature found for AgNP biosynthesis was 35°C and 45°C (Figure 3C). Absorbance values also increased with time, up to 64 h, but did not increase thereafter (Figure 3D). The effect of $AgNO_3$ concentrations on AgNPs formation is shown in Fig. 3C. Increasing levels of AgNPs formation were observed with an increasing $AgNO_3$ concentration. The highest AgNPs were obtained from 0.25 mM $AgNO_3$ concentration.

Characterization of Silver Nanoparticles

FTIR analysis of the synthesized AgNPs revealed visible bands at 3425.58, ~2920, 2858.51, 2355.08, 1647.21, 1556.55, 1456.26, 1382.96, and 1068.56 cm^{-1}, as shown in Fig. 4. The band seen at 3425.58 cm^{-1} can be attributed to O–H (alcohol) stretching. Two peaks are attributed to C–H (alkane) stretching which is

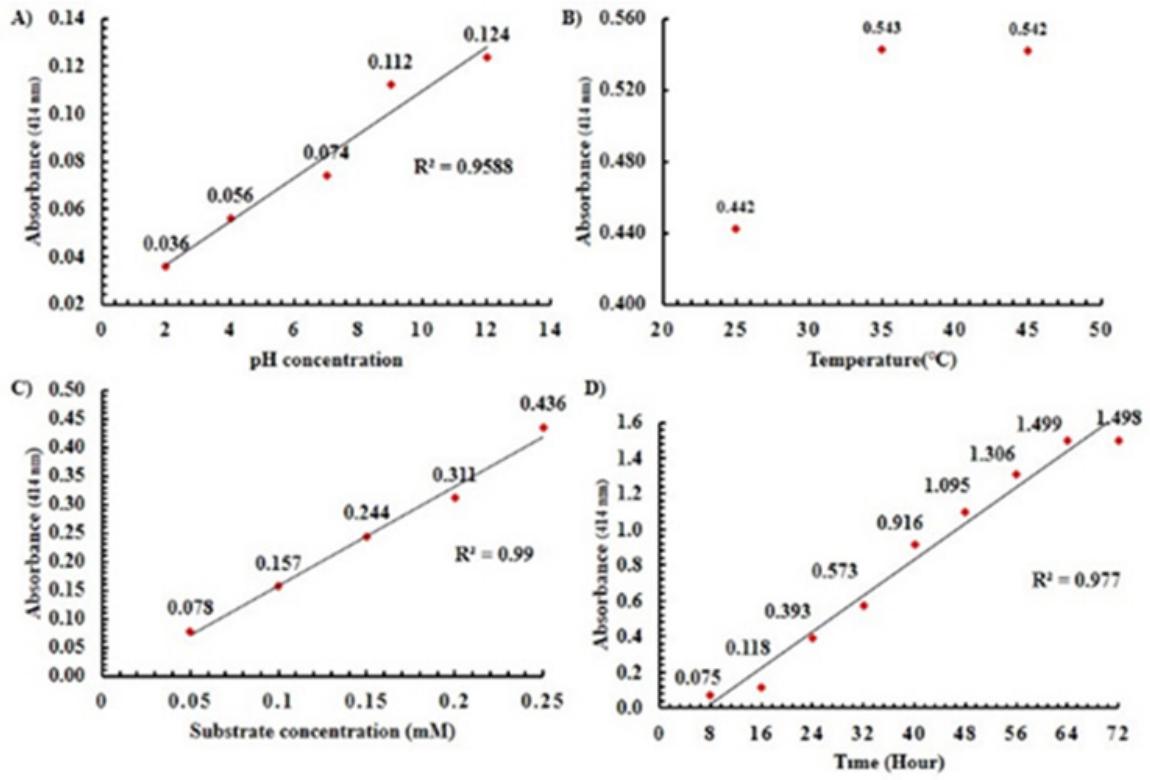

Figure 3. Effect of pH (A), temperature (B), substrate concentration (C), and exposure periods (D) on the substrate on the stability of AgNPs synthesis.

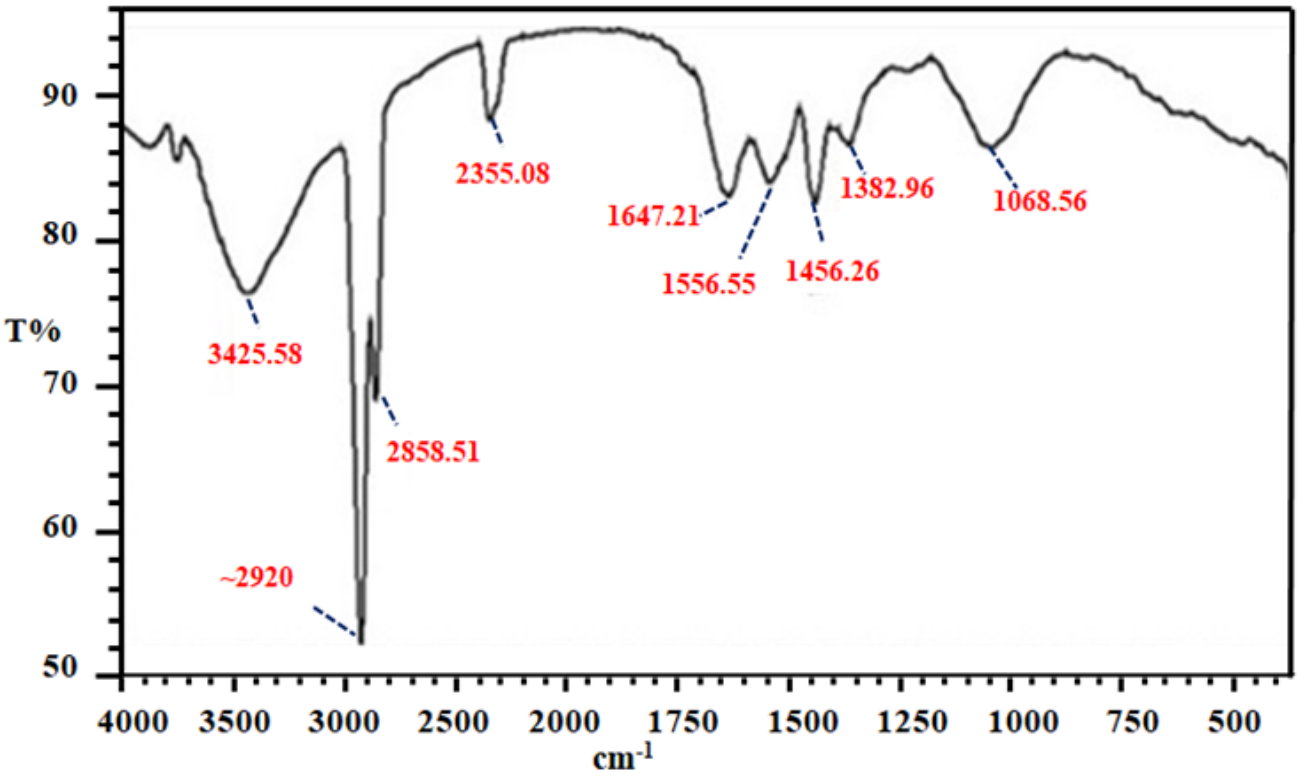

Figure 4. FTIR spectrum of green synthesized AgNPs

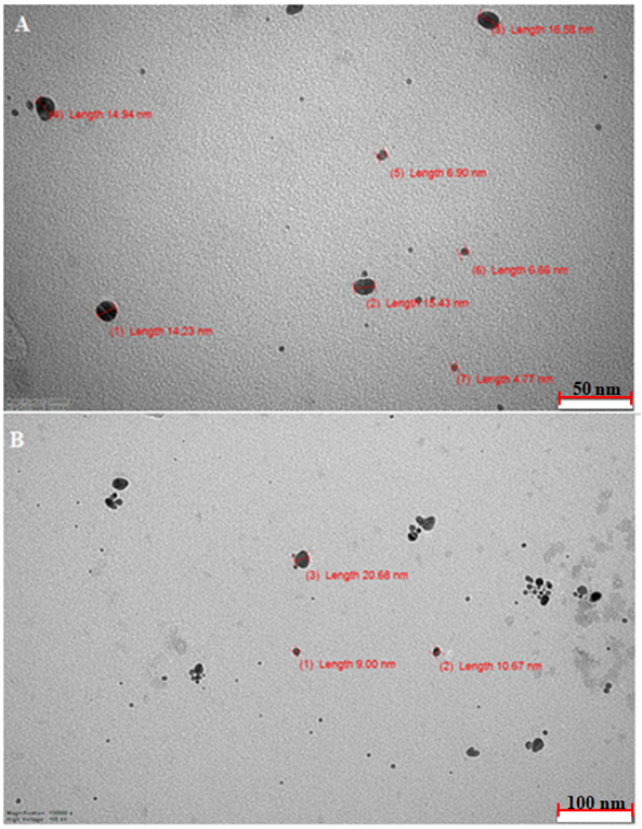

Figure 5. TEM images of AgNPs for scale bar of a) 50 nm b) 100 nm.

Table 1. Antimicrobial activity of CFF, $AgNO_3$, and AgNPs.

Agents		Diameter zone (mm) ± Standard Deviation			
		S. aureus ATCC 25923	*P. aeruginosa* ATCC 27853	*E. coli* ATCCC 25922	*B. subtilis*
Vancomycin (30 µg)		21±2	8.67±0.58	25±1	22±1.73
Penicillin (10 µg)		41±3	Not determined	33.67±0.58	30.67±2.08
Chloramphenicol (30 µg)		26.67±0.58	16±1.73	30.33±1.53	36±1.73
Erythromycin (15 µg)		30.33±2.08	9±1	26.67±1.53	29±1
Tetracycline (30 µg)		30.33±2.52	14.67±0.58	11.67±0.58	16±2
Cell-Free Filtrate		0	0	0	0
Ag NO3 2,5 mM		18.33±1.53	13±1	14.33±1.15	16.33±1.53
AgNPs	10 ppm	10±1.73	12.33±1.53	12.33±1.53	17± 1
	1 ppm	9±1	11±1.73	0	16.33± 2.08
	0.1 ppm	0	0	0	8.33±0.58

observed at ~2920 and 2858.51 cm^{-1}. A further band observed at 2355.08 cm^{-1} represents the H-C=O (aldehyde hydrogen) stretching. When analyzing the FTIR spectra, it was seen that the stretching vibrations of the amide I and amide II bands of the proteins were at 1647.2 cm^{-1}. The last band, which was seen at 1068.56 cm^{-1}, is accounted for by C–O (alcohol/ether) stretching. FTIR data exhibit that the biological compounds or molecules can be preferred for both stabilization and synthesis of AgNPs.

The TEM image of synthesized AgNPs displayed small particles with clear morphology. Figure 5a (scale bar of 50 nm) and Figure 5b (scale bar of 100 nm) present TEM images of AgNPs for two different scale bars. TEM analysis demonstrated the spherical shape of synthesized silver nanoparticles; these ranged in size from 4.77 nm to 20.68 nm with an average length of 11.88±5.06 nm.

Table 2. Biofilm inhibition (%) of AgNPs against *P. aeruginosa* ATCC 27853

	AgNPs		
Inhibition % (n=3)	10 ppm	1 ppm	0.1 ppm
	81.13	67.63	40.28
	76.25	65.45	45.11
	80.62	63.32	40.43
Average biofilm inhibition (%) ± Standard Deviation	79.33±2.68	65.47±2.16	41.94±2.75

Table 3. Genotoxic evaluation of $AgNO_3$ and AgNPs using SMART assay

Treatments	Number of Wings (N)	Small uniform clones (1-2 cells) (m=2)			Large uniform clones (> 2 cells) (m=5)			Twin clones (m=5)			Total mwh clones (m=2)			Total clones (m=2)		
		No.	Fr.	D.	No.	Fr.	D.	No.	Fr.	D.	No.	Fr.	D.	No.	Fr.	D.
Normal Wing																
Distilled Water	80	12	(0.16)		2	(0.02)		0	(0.00)		13	(0.19)		14	(0.19)	0.76
1 mM EMS	31	69	(2.21)	+	27	(0.83)	+	9	(0.27)	+	105	(3.31)	+	104	(3.40)	+ 5.38
$AgNO_3$ (ppm)																
0.1	80	15	(0.16)	i	5	(0.06)	i	0	(0.00)	i	20	(0.25)	i	20	(0.25)	i 1.02
1	80	9	(0.07)	-	2	(0.02)	i	0	(0.00)	-	8	(0.10)	-	11	(0.10)	- 0.41
10	80	5	(0.01)	-	2	(0.02)	i	0	(0.00)	-	3	(0.03)	-	7	(0.03)	- 0.15
AgNPs (ppm)																
0.1	80	15	(0.16)	i	5	(0.06)	i	0	(0.00)	i	20	(0.25)	i	20	(0.25)	i 1.02
1	80	6	(0.05)	-	2	(0.02)	i	0	(0.00)	-	8	(0.8)	-	8	(0.8)	- 0.39
10	80	4	(0.01)	-	2	(0.02)	i	0	(0.00)	-	3	(0.03)	-	6	(0.03)	- 0.15

EMS.. Ethyl methanesulfonate; Fr.. frequency; D.. display of statistics results; +.. positive; -.. negative; i.. trivial difference; m..multiplication factor; probability level = 0.05

The average diameter obtained for AgNPs in ultrahigh-purity water suspension is in the size distribution of between 32.5 and 75.6 nm with a mean diameter of 55.15±14.83 nm for silver nanoparticles. The obtained PdI value of AgNPs was 0.185. Zeta potential and electrophoretic mobility of AgNPs were defined as –19.38±0.73 mV and -1.51±0.06 µm cm/sV, respectively. This zeta potential and electrophoretic mobility results are reported as an average value of three measurements.

The antibacterial activity of the AgNPs

The fungal AgNPs have been tested for antibacterial activity against *E.coli* (ATCC 25922), *P. aerouginosa* ATCC 27853 (Gram-negative), and *B. subtilis*, *S. aureus* ATCC 25923 (Gram-positive). Testing for antimicrobial activity showed that the synthesized AgNPs had antimicrobial activity on all the tested bacteria except *E. coli* in a dose-dependent manner (Table 1). CFF did not show antimicrobial effects on gram-positive and negative bacteria. 0.25 mM $AgNO_3$ showed antimicrobial effects on all tested bacteria. 10 ppm AgNPs showed more antibacterial effects (12.33±1.53) than Vancomycin (8.67±0.58) and Erythromycin (9±1) on *P. aeruginosa*. 10 ppm (17± 1) and 1 ppm (16.33± 2.08) concentrations of AgNPs showed more antimicrobial effects than Tetracycline (16±2) on *B. subtilis*.

Biofilm inhibition of AgNPs

That fungal synthesized AgNPs can effectively inhibit biofilms formed by *P. aeruginosa* in a dose-dependent manner has been demonstrated; 79.33, 65.47, and 41.95% decrease in biofilm was observed at 10, 1, and 0.1 ppm, respectively (Table 2).

Drosophila melanogaster Somatic Mutation and Recombination Test (SMART)

$AgNO_3$ and AgNPs (0.1, 1, and 10 ppm) whose genotoxic properties are evaluated with SMART, as shown in Table 3. 72±4 h 3rd stage trans-heterozygous larvae were exposed to 3 different concentrations (0.1, 1, 10 ppm) of $AgNO_3$ and AgNPs, distilled water (negative control) and 1mM of Ethyl methanesulfonate (positive control). In the evaluating genotoxic effects of $AgNO_3$ and AgNPs, wing preparations were prepared from normal poultry individuals for each concentration. In 72±4 h distilled water application, a total of 14 clones were determined, including 12 small uniform clones and 2 large uniform clones in 80 wings. Additionally, the total number of mwh clones found was 13. In distilled water application, clone induction frequency was calculated to be 0.76. Comparing the results obtained from the application of different concentrations of $AgNO_3$ and AgNPs and those obtained from the control group application of distilled water, it was observed that there was no statistically significant difference between any of the clone types. The results for EMS applications used as positive control were compared with those for distilled water applications, and in all clone types, a positive reaction was observed. Neither increase nor decrease was seen in the total clone induction frequency at a specific rate depending on the dose increase. The obtained application results for all concentrations showed that the differences were not statistically significant compared with those obtained from the distilled water, which is the wing preparations, the control group.

Discussion

Extracellular biosynthesis of AgNPs is a method that uses a cell-free fungi filtrate as the reducing agent (33) and is both environmentally friendly and energy-efficient. In this study, the extracellular synthesis of AgNPs using *N. clavispora* was determined by the UV-vis spectrophotometer (Fig 2). The color of the CFF transitioned from a light yellow to a dark brown due to the reduction of the silver ion. This is the first indication of the fungal synthesis of AgNPs (Fig. 2). AgNPs are able to be synthesized after the reduction of silver nitrate solution using cell filtrates of *Phoma glomerata*, *Aspergillus terreus*, *Penicillium notatum*, *Phanerochaete chrysosporium*, *Trichoderma asperellum*, and *A. clavatus* (34-37). The aforementioned color change is presumably related to the excitement of the Surface Plasmon Resonance (SPR) bands of the AgNPs (38-39). The synthesized AgNPs showed an SPR peak observed in the range of 400-450 nm (40). Similarly, the bands were observed in the wavelength of 414 nm, which is typical for AgNPs (Fig 2), in agreement with other AgNPs syntheses from biological sources (41-46).

In the stabilization and accumulation of the particles, the optimization phase plays a crucial role. By regulating parameters such as pH, temperature, the concentration of the substrate, and exposure period, the size of nanoparticles is controllable (47). Different fungi and conditions can be utilized to generate various AgNPs (48). The stability of AgNPs, on the other hand, remains a challenge to control; biosynthesis efficiency is additionally reportedly very limited (49). The methods making use of biomass extracted from the reaction medium produced more AgNPs, but also a narrower AgNPs size range (1.5–20 nm) in comparison to those solutions that used biomass and biomass filtrates (50). Researchers have attempted to optimize the conditions to control the yield, scale, and properties of fungal AgNPs (51). Fig. 3A shows that the synthesis of fungal AgNPs increased with an increase in pH; high absorption values were observed via spectrophotometer at pH 12. Nanoparticle synthesis increase is possible at alkaline pH values, due to competition for the creation of negatively charged bonds between proton and metal ions (52). With the use of citrate-capped AgNPs, there has been observed a linear correlation between pH and the concentration of generated AgNPs (53). Our FTIR data show that the biological compounds can be capped fungal AgNPs. Maximum AgNPs production was observed between pH 9 and 11 for *Fusarium oxysporum* (54), at pH 12 for *Sclerotinia sclerotiorum* MTCC 8785 (55), and *Penicillium oxalicum* (6).

High absorption values in the spectrophotometer for AgNPs were observed at 35°C and 45 °C (Fig. 3B). Similar to our results, the optimum temperature for fungus mediated AgNPs was observed at 40 °C for *Trichoderma harzianum* (56) and *Rhizopopus stonolifer* (57), at 50 °C for *Fusarium oxysporium* (54), and at 30 °C for *Guignardia mangifera* (58). The temperature degrees used in the synthesis of fungal AgNPs can affect the synthesis rate, the size, and the stability of the NPs (59). AgNPs formation increased by increasing $AgNO_3$ concentration (Fig. 3C.). The highest AgNPs were obtained from a 0.25 mM concentration of $AgNO_3$. 0.25 mM $AgNO_3$ was selected for AgNPs production to obtain well-dispersed small nanoparticles because high $AgNO_3$ concentrations can produce large nanoparticles with irregular morphological features (60). In addition, the toxicity of the AgNPs may increase with increasing $AgNO_3$ concentration (57). Absorbance values also increased with time, up to 64 h, but did not increase thereafter (Figure 3D). Ottoni et al. (61) reported that the maximum AgNPs absorption values were determined at 72 h.

Extracellularly formed nanoparticles have been stabilized with proteins and reducing agents secreted by the fungus. In total, four high molecular weight proteins produced from fungal biomass have been reported in combination with nanoparticles. Furthermore, removing metal ions and the surface attachment of proteins to nanoparticles did not weaken the tertiary structure of proteins (62). The compounds of aliphatic and aromatic hydrocarbons comprise a broad variety of functional groups, (–CN, –SH, –COOH, $–NH_2$); these are reported to have a strong propensity for the functionalization of noble metal nanoparticles, rendering them valuable as surface-protective functional groups (63-68). Carbonyl bound in peptide-protein residues and amino acid has been confirmed to have a larger capacity to bind metals, to the extent that proteins form a coating covering the metal nanoparticles to prevent and stabilize the agglomeration of particles. From this, we can surmise that proteins can be attached to nanoparticle surfaces via free amine groups or cysteine residues which will act as encapsulating agents and stabilize particles. FTIR data demonstrate that the

biological compounds or molecules can be preferred for both stabilization and synthesis of AgNPs (Figure 4).

TEM images of synthesized AgNPs displayed the tiny particles with clear morphology. TEM analysis demonstrated a spherical shape of synthesized silver nanoparticles. The average nanoparticle size was determined as 11.88±5.06 nm (Figure 5). The obtained average diameter for AgNPs in ultrahigh-purity water suspension presents a distribution of values ranging between 32.5 and 75.6 nm with a mean diameter of 55.15±14.83 nm for silver nanoparticles. Furthermore, the PdI value of AgNPs in ultrahigh-purity water suspension was obtained as 0.185. Zeta potential (ζ) and electrophoretic mobility of AgNPs in ultrahigh-purity water were found as –19.38±0.73 mV and -1.51±0.06 μm cm/sV. Electrophoretic mobility for AgNPs was calculated by Henry's equation (69). Similar studies have been carried out using the extracellular CFF of *Punctularia atropurpurascens*, *Penicillium expansum*, and *Phanerochaete chrysosporium* fungi to produce SNPs. The size distribution and average sizes of PaNPs, PeNPs, and PchNPs were observed between 12 nm-30 nm, and between 11 nm-38 nm via DLS and TEM, respectively. When the average sizes of these three nanoparticles were compared with the data obtained from our current study, the comparison showed consistency of results; the average diameter of AgNP synthesized using *N. clavispora* was observed less than 50 nm. In addition, PDI values of this fungus was consistent with the PDI value of *N. clavispora* silver nanoparticles as < 0.4 (70). Zeta potential value displays the negative charge of synthesized AgNPs (-20.1 mV) in our current study; this value is close to the zeta potential value (-18.5 mV) of AgNPs that were biosynthesized using aqueous leaf extracts of Eichhornia crassipes as previously presented by Heikal et al. (71). These high negative potential values can support improving the high colloidal nature and dispersity of AgNPs because of negative repulsion (72).

The antimicrobial action of Ag+ is thought to be exhibited through the absorption of ions by the microorganism cell, along with an accumulation within the cell leading to a shrinkage of the cytoplasm membrane or the attraction of the cytoplasm to itself by the cell wall. It is reported that in this way DNA molecules are damaged, and cells lose their ability to replicate due to the infiltration of Ag+. Furthermore, Ag+ has been shown to act upon the -SH bonds of proteins and cause them to be inactivated (73). Cho et al. (74) reported that silver clumps act as a catalyst for the oxidation of microorganisms in oxygen-added solutions. Antimicrobial activity results showed that synthesized AgNPs possessed antimicrobial activity on all the tested bacteria except *E. coli*, in a dose-dependent manner (Table 1). The antibacterial mechanism of AgNPs has only tentative explanations. According to some studies, gram-negative bacteria show more sensitivity to AgNPs compared to gram-positive bacteria (9,75), while other research reports the reverse (76,77). However, it is known that the antimicrobial activity depends on the type of microbial species and the concentration of AgNPs (78-81). It has been further observed elsewhere that AgNPs resistance in the *E. coli* K-12 MG1655 strain can develop rapidly, with relatively few mutational steps. This does not bode well for the prospect of continuous use of AgNPs as antimicrobial agents (82). After repeated exposure to silver nanoparticles, Gram-negative bacteria as *Escherichia coli* 013, *Pseudomonas aeruginosa* CCM 3955, and *E. coli* CCM 3954 were all able to develop resistance to the antimicrobial effect. This resistance is caused by the production of the adhesive flagellum protein flagellin, which in turn causes the nanoparticles to clump together. The resistance develops without requiring any genetic changes; what is required is only a phenotypic modification, to reduce the colloidal stability of the nanoparticles and thus eradicate their antibacterial activity (83).

We have demonstrated that fungal synthesized AgNPs can be effective for the inhibition of biofilms formed by *P. aeruginosa* in a dose-dependent manner. 79.33, 65.47, and 41.95% decrease in biofilm was observed at 10, 1, and 0.1 ppm, respectively (Table 2). According to the literature, AgNPs have a good effect on the biofilm layer formed by bacteria due to their large surface areas. AgNPs interact with sulfuric compounds in the bacterial cell membrane, phosphorus-containing compounds in protein, and DNA. AgNPs have a strong antibiofilm effect against *Pseudomonas putida*, *P. aeruginosa*, *S. aureus*, *Shigella flexneri*, *Staphylococcus epidermidis*, *Streptococcus pneumonia*, and *E.coli* (84-87).

D. melanogaster has orthologs of approximately 65–80 % of human genes (88). SMART results did not indicate any mutagenic effect against *D. melanogaster* used for screening the mutagenicity of the biogenic AgNPs; they were found to be genotoxicity safe. Avalos et al. (89) investigated the AgNPs' toxicity of different sizes by the *Drosophila* SMART and found a statistically insignificant low toxicity. AgNPs showed toxic effects in mammalian and human cells such as liver macrophages (90) and epithelial cells (91). In contrast, it was demonstrated that AgNPs accumulated in liver, lung, kidney, stomach, testicle, and brain cells but did not show a significant genotoxicity function (91). AgNPs successfully killed microorganisms without inducing any cytotoxicities and were found to be nontoxic when delivered through nasal, ocular, and dermal pathways (59,92). Kevin et al. (93) discovered a negative correlation between the toxicity of AgNPs and tissue Ag concentration and further that there was no relationship with dissolved Ag concentration in test media. This comparison demonstrates the difficulty of generalizing the toxic mechanisms of AgNPs toxic across different species and life stages. Furthermore, decreased toxicity has been reported in encapsulated fungal nanoparticles (94,95). Endocytosis into an endosome and then into a lysosome are the first steps of AgNPs entering the cell (96). They are faced with acidic conditions, with pH values ranging between 4 to 5.34 (97). With lower pH, the release of Ag from AgNPs increases. This expertise could assist in reducing AgNPs toxicity; biogenic synthesis, utilizing nontoxic reagents obtained from biological materials, therefore is an exciting alternate technological route for metal nanoparticles (95). In this study, FTIR analysis showed that biological molecules could be involved in both the synthesis and the stabilization of AgNPs (Fig 4).

Conclusion

AgNPs were synthesized for the first time using CFF of *N. clavispora* MH244410.1 and characterized by several important types of equipment. The average diameter of the AgNPs was potential and electrophoretic mobility of AgNPs was defined as –19.38±0.73 mV and -1.51±0.06 µm cm/sV, respectively. Experimental results obtained for the characterization of AgNPs are in good agreement with the literature's values. The synthesized AgNPs showed antibacterial activity against *S. aureus*, *P. aeruginosa*, and *B.subtilis*. SMART results did not indicate any mutagenic effect against *D. Melanogaster*. 79.33, 65.47, and 41.95% inhibition of biofilms formed by *P. aeruginosa* were observed at 10, 1, and 0.1 ppm of AgNPs, respectively. The nano-sized AgNPs have unique advantages and a wide range of applications that have been proved by a large number of reports (36,75,98,99). Our FTIR data results illuminate that the biological compounds or molecules can be preferred for both stabilization and synthesis of AgNPs. More studies are needed on the synthesis mechanism of AgNPs and extracellular AgNP synthesis. Secondary metabolites that can cause changes in cytotoxicity and antimicrobial properties when AgNPs are obtained using extracellular methods should be identified, especially in future studies.

Acknowledgment

The authors wish to thank Syed Hasan Ali Ahmed, Swansea-the UK, for editing the language of the paper.

Conflict of interest

None

References

1. Tan S, Erol M, Attygalle A, Du H, Sukhishvili S. Synthesis of positively charged silver nanoparticles via photoreduction of AgNO3 in branched polyethyleneimine/HEPES solutions. Langmuir 2007; 23: 9836–9843.
2. Krishnan V, Kamala Nalini S.P. Biotemplates in the green synthesis of silver nanoparticles. Biotechnol. J. 2010; 5: 1098–1110.
3. Osonga FJ, Kalra S, Miller RM, Isikab D, Sadik OA. Synthesis, characterization and antifungal activities of eco-friendly palladium nanoparticles. RSC Adv 2020; 10: 5894–5904.
4. Gade AK, Bonde P, Ingle AP, Marcato PD, Durán N, Rai MK. Exploitation of *Aspergillus niger* for synthesis of silver nanoparticles. J Biobased Mater Bioenergy 2008; 2: 243–247.
5. Balaji DS, Basavaraja S, Deshpande R, BedreMahesh D, Prabhakar BK, Venkataraman A. Extracellular biosynthesis of functionalized silver nanoparticles by strains of *Cladosporium cladosporioides* fungus. Colloids Surf B Biointerfaces 2009; 68(1): 88-92.
6. Du L, Xu Q, Huang M, Xian L, Feng, JX. Synthesis of small silver nanoparticles under light radiation by fungus *Penicillium oxalicum* and its application for the catalytic reduction of methylene blue. Mater Chem Phys 2015; 160: 40–47.
7. Reddy NV, Satyanarayana BM, Bobbu P, Bhaskar BV, Aishwarya S, Venkateswara RJ, Vijaya T. Biogenesis of silver nanoparticles using endophytic fungus *Pestalotiopsis microspora* and evaluation of their antioxidant and anticancer activities. Int J Nanomedicine 2016; 11: 5683-5696.
8. Velusamy P, Kumar GV, Jeyanthi V, Das J, Pachaiappan R. Bio-inspired green nanoparticles: synthesis, mechanism, and antibacterial application. Toxicol Res 2016; 32: 95–102.
9. Casagrande MG, de Lima R. Synthesis of silver nanoparticles mediated by fungi: a review. Front Bioeng Biotechnol 2019; 7: 1-16.
10. Yahyaei B, Pourali P. One step conjugation of some chemotherapeutic drugs to the biologically produced gold nanoparticles and assessment of their anticancer effects. Sci Rep 2019; 9: 10242.
11. Jaidev LR, Narasimha G. Fungal mediated biosynthesis of silver nanoparticles, characterization and antimicrobial activity. Colloids Surf B Biointerfaces 2010; 81(2): 430–433.
12. El-Sonbaty SM. Fungus-mediated synthesis of silver nanoparticles and evaluation of antitumor activity. Cancer Nanotechnol 2013; 4(4–5): 73–79.
13. Prakash P, Gnanaprakasam P, Emmanuel R, Arokiyaraj S, Saravanan M. Green synthesis of silver nanoparticles from leaf extract of *Mimusops elengi*, Linn. for enhanced antibacterial activity against multi drug resistant clinical isolates. Colloids Surf B 2013; 108: 255–259.
14. Elgorban AM, Aref SM, Seham SM, Elhindi KM, Bahkali AH, Sayed SR, Manal MA. Extracellular synthesis of silver nanoparticles using *Aspergillus versicolor* and evaluation of their activity on plant pathogenic fungi. Mycosphere 2016; 7(6): 844–852.
15. Barabadi H, Honary S, Ebrahimi P, Alizadeh A, Naghibi F, Saravanan M. Optimization of myco-synthesized silver nanoparticles by response surface methodology employing Box-Behnken design. Inorg Nano-Met Chem 2019; 49(2): 33- 43.
16. Xu, J, Ebada SS, Proksch P. Pestalotiopsis a highly creative genus: chemistry and bioactivity of secondary metabolites Fungal Divers 2010; 44: 15-31.
17. Xu J, Yang X, Lin Q. Chemistry and biology of Pestalotiopsis-derived natural products. Fungal Divers 2014; 66: 37-68.
18. Maharachchikumbura SSN, Guo LD, Cai L, Chukeatirote E, Wu VP, Sun X, Crous PW, Bhat DJ, McKenzie EHJ, Bahkali AH, Hyde KH. A multi-locus backbone tree for Pestalotiopsis, with a polyphasic characterization of 14 new species. Fungal Divers 2012; 56: 95-129.
19. Strobel G, Ford E, Worapong J, Harper JK, Arif AM, Grant DM, Fung PCW, Chau RMW. Ispoestacin, an isobenzofuranone from *Pestalotiopsis microspora*, possessing antifungal and antioxidant activities. Phytochemistry 2002;

60: 179–183.
20. Ding G, Li Y, Fu S, Liu S, Wei J, Che Y. Ambuic acid and torreyanic acid derivatives from the endolichenic fungus *Pestalotiopsis sp*. J Nat Prod 2009; 72: 182–186.
21. Netala VR, Bethu MS, Pushpalatha B, Baki VB., Aishwarya S, Rao JV, Tartte V. Biogenesis of silver nanoparticles using endophytic fungus *Pestalotiopsis microspora* and evaluation of their antioxidant and anticancer activities. Int J Nanomedicine 2016; 11: 5683-5696.
22. Hassan SH, Koutb M, Nafady NA, Hassan EA. Potentiality of *Neopestalotiopsis clavispora* ASU1 in biosorption of cadmium and zinc. Chemosphere 2018; 202: 750-756.
23. Biju CN, Peeran MF, Gowri R. Identification and characterization of *Neopestalotiopsis clavispora* associated with leaf blight of small cardamom (*Elettaria cardamomum* Maton). J Phytopathol 2018; 166: 532–546.
24. Gardes M, Bruns TD. ITS primers with enhanced specificity for basidiomycetes—Application to identification of mycorhizae and rusts. Mol Ecol 1993; 2(2): 113-118.
25. Maliszewska I, Szewczyk K, Waszak K. Biological synthesis of silver nanoparticles. J Phys Conf Ser 2009; 146: 012025.
26. Sobhy II, Hafez A, Nafady NA, Abdel-Rahim IR, Shaltout AM, Mohamed MA. Biogenesis and optimisation of silver nanoparticles by the endophytic fungus *Cladosporium sphaerospermum*. Int J Nano Chem 2016; 2(1): 11-19.
27. Roy S, Mukherjee T, Chakraborty S, Das TK. Biosynthesis, characterisation & antifungal activity of silver nanoparticles synthesized by the fungus *Aspergillus foetidus* MTCC8876. Dig J Nanomater Biostruct 2013; 8(1): 197-205.
28. Jahangırıan H, Haron, MDJ, Ismail MHS, Moghaddam RR, Hejri LA, Abdollahi Y, Rezayi M, Vafaei N. Well diffusion method for evaluation of antibacterial activity of copper phenyl fatty hydroxamate synthesized from canola and palm kernel oils. Dig J Nanomater Biostruct 2013; 8(3): 1263-1270.
29. Sandberg M, Maattanen A, Peltonen J, Vuorela PM, Fallarero A. Automating a 96-well microtitre plate model for *Staphylococcus aureus* biofilms: an approach to screening of natural antimicrobial compounds. Int J Antimicrob Agents 2008; 32: 233-240.
30. Lindsley DL, Zimm GG. The genome of *Drosophila melanogaster*. Academic Press, San Diego, California 1992
31. Graf U, Wurgler FE, Katz AJ, Frei H, Juan H, Hall CB, Kale PG. Somatic mutation and recombination test in *Drosophila melanogaster*. Environ Mutagen 1984; 6: 153-188.
32. Kastenbaum MA, Bowman KO. Tables for determining the statistical significance of mutation frequencies. Mutation Res 1970; 9: 527-549.
33. Narayanan KB, Sakthivel N. Biological synthesis of metal nanoparticles by microbes. Adv Colloid Interf Sci 2010; 156: 1-13.
34. Vigneshwaran N, Kathe AA, Varadarajan PV, Nachane RP, Balasubramanya RH. Biomimetics of silver nanoparticles by white rot fungus, *Phaenerochaete chrysosporium*. Colloids Surf B Biointerfaces 2006; 53: 55–59.
35. Birla SS, Tiwari VV, Gade AK, Ingle AP, Yadav MKR. Fabrication of silver nanoparticles by *Phoma glomerata* and its combined effect against *Escherichia coli*, *Pseudomonas aeruginosa* and *Staphylococcus aureus*. Lett Appl Microbiol 2009; 48: 173-179.
36. Li GQ, He D, Qian YQ, Guan B, Gao S, Cui Y, Yokoyama K, Wang L. Fungus-mediated green synthesis of silver nanoparticles using *Aspergillus terreus*. Int J Mol Sci 2012; 13: 466-476.
37. Manjunath HMJC, Raju NG. Synthesis and biological evaluation of anti-tubercular activity of some synthesised pyrazole derivatives. J Chem Pharm Res 2014; 6: 112-117.
38. Hamedi S, Shojaosadati SA, Shokrollahzadeh S, Hashemi-Najafabadi S. Extracellular biosynthesis of silver nanoparticles using a novel and non-pathogenic fungus, *Neurospora intermedia*: controlled synthesis and antibacterial activity. World J Microbiol Biotechnol 2014; 30: 693-704.
39. Sadeghi B, Gholamhoseinpoor F. A study on stability and green synthesis of silver nanoparticles using *Ziziphora tenuior* (Zt) extract at room temperature. Spectrochim Acta Part A: Mol Biomol Spectrosc 2015; 134: 310-315.
40. Sastry M, Mayyaa KS, Bandyopadhyay K. pH dependent changes in the optical properties of carboxylic acid derivatized silver colloid particles. Colloid Surf A 1997; 127: 221-228 .
41. Hiremath J, Rathod V, Ninganagouda S, Singh D, Prema K. Antibacterial activity of silver nanoparticles from rhizopus spp against gram negative *E. coli* MDR strains. J Pure Appl Microbio 2014; 8(1): 555-562.
42. Varadavenkatesan T, Selvaraj R, Vinayagam R. Phyto-synthesis of silver nanoparticles from *Mussaenda erythrophylla* leaf extract and their application in catalytic degradation of methyl orange dye. J Mol Liq 2016; 221: 1063-1070.
43. Ghiuță I, Cristea D, Croitoru C, Kost J, Wenkert R, Vyrides A, Anayiotos A, Munteanu D. Characterization and antimicrobial activity of silver nanoparticles, biosynthesized using Bacillus species. Appl Surf Sci 2018; 438: 66–73.
44. Halawani EM. Rapid biosynthesis method and characterization of silver nanoparticles using *Zizyphus spina* christi leaf extract and their antibacterial efficacy in therapeutic application. J Biomater Nanobiotechnol 2016; 8(1): 22-35.
45. Tyagi S, Tyagi PK, Gola D, Chauhan N, Bharti RK. Extracellular synthesis of silver nanoparticles using entomopathogenic fungus: characterization and antibacterial potential. SN Applied Sciences 2019; 1: 1545
46. Kumari RM, Kumar V, Kumar M, Pareek N, Nimesh S. Assessment of antibacterial and anticancer capability of silver nanoparticles extracellularly biosynthesized using *Aspergillus terreus*. Nano Express 2020; 1(3), 030011.
47. Gericke M, Pinches A. Biological synthesis of metal nanoparticles. Hydrometallurgy 2006; 83: 132-140.
48. Devanesan S, AlSalhi MS, Vishnubalaji R, Alfuraydi AA, Alajez NM, Alfayez M, Murugan K, Sayed SRM, Nicoletti

M, Benelli G. Rapid biological synthesis of silver nanoparticles using plant seed extracts and their cytotoxicity on colorectal cancer cell lines. J Clus Sci 2017; 28: 595–605.
49. Murali MY, Vimala K, Thomas V, Varaprasad K, Sreedhar B, Bajpai SK, Mohana Raju K. Controlling of silver nanoparticles structure by hydrogel networks. J Colloid Interface Sci 2010; 342: 73–82.
50. Zahran MK, Mohamed AA, Mohamed FM, El-Rafie MH. Optimization of biological synthesis of silver nanoparticles by some yeast fungi. Egypt J Chem 2013; 56: 91-110.
51. Ma L, Su W, Liu JX, Xi Zeng X, Huang Z, Li W, Liu ZC, Tang JX. Optimization for extracellular biosynthesis of silver nanoparticles by *Penicillium aculeatum* Su1 and their antimicrobial activity and cytotoxic effect compared with silver ions. Mater Sci Eng C 2017; 77: 963–971.
52. Sintubin L, Windt WD, Dick J, Mast J, Ha DVD, Verstraete W, Boon N. Lactic acid bacteria as reducing and capping agent for the fast and efficient production of silver nanoparticles. Appl Microbiol Biotechnol 2009; 84: 741–749.
53. Contreras-Trigo B, Díaz-García V, Guzmán-Gutierrez E, Sanhueza I, Coelho P, Godoy SE, Sergio T, Oyarzún P. Slight pH fluctuations in the gold nanoparticle synthesis process influence the performance of the citrate reduction method. Sensors 2018; 18: 2246.
54. Birla SS, Gaikwad SC, Gade AK, Rai MK. Rapid synthesis of silver nanoparticles from *Fusarium oxysporum* by optimizing physicocultural conditions. Sci World J 2013; 796018
55. Juhi S, Sharma PK, Sharma MM, Singh A. Process optimization for green synthesis of silver nanoparticles by *Sclerotinia sclerotiorum* MTCC 8785 and evaluation of ıts antibacterial properties. Springerplus 2016; 5(1): 861
56. Ahluwalia V, Kumar J, Sisodia R, Shakil NA, Walia S. Green synthesis of silver nanoparticles by *Trichoderma harzianum* and their bio-efficacy evaluation against *Staphylococcus aureus* and *Klebsiella pneumonia*. Ind Crops Prod 2014; 55: 202–206.
57. AbdelRahim K, Mahmoud SY, Ali AM, Almaary KS, Mustafa AEZMA, Husseiny SM. Extracellular biosynthesis of silver nanoparticles using *Rhizopus stolonifer*. Saudi J. Biol. Sci. 2017; 24: 208-216.
58. Banu AN, Balasubramanian C. Optimization and synthesis of silver nanoparticles using *Isaria fumosorosea* against human vector mosquitoes. Parasitol Res 2014; 113: 3843-3851.
59. Elamawi RM, Raida E, Al-Harbi Awatif A. Biosynthesis and characterization of silver nanoparticles using *Trichoderma longibrachiatum* and their effect on phytopathogenic fungi. Egypt J Biol Pest Control 2018; 28: 28.
60. Balakumaran MD, Ramachandran R, Kalaicheilvan PT. Exploitation of endophytic fungus, *Guignardia mangifera*e for extracellular synthesis of silver nanoparticles and their in vitro biological activities. Microbiol Res 2015; 178: 9-17.
61. Ottoni CA, Simões MF, Fernandes S, Gomes dos Santos J, Sabino da Silva E, Brambilla de Souza RF, Maiorano AE. Screening of filamentous fungi for antimicrobial silver nanoparticles synthesis. AMB Expr 2017; 7: 31.
62. Mohanpuria P, Nisha KR, Yadav SK. Biosynthesis of nanoparticles: technological concepts and future applications. J Nanopart Res 2008; 10: 507-517.
63. Laibinis PE, Whitesides GM. Self-Assembled monolayers of n- alkanethiolates on copper are barrier films that protect the metal against oxidation by air. J Am Chem Soc 1992; 114: 9022-9028.
64. Teranishi T, Kiyokawa I, Miyake M. Synthesis of monodisperse gold nanoparticles using linear polymers as protective agents. Adv Mater 1998; 10: 596-599.
65. Teranishi T, Hosoe M, Tanaka T, Miyake M. Size control of monodispersed Pt nanoparticles and their 2D organization by electrophoretic deposition. J Phys Chem B 1999; 103: 3818-3827.
66. Corbierre MK, Cameron NS, Sutton M, Mochrie SG, Lurio LB, Rühm A, Lennox RB. Polymer-stabilized gold nanoparticles and their incorporation into polymer matrices. J Am Chem Soc 2001; 123: 10411-10412.
67. Mandal TK, Fleming MS, Walt DR, Preparation of polymer couted gold nanoparticles by surface-confined radical polymerization at ambient temperature. Nano Lett 2002; 2: 3–7.
68. Shan J, Nuopponen M, Jiang H, Kauppinen E, Tenhu H. Preparation of poly(n-isopropylacrylamide)-monolayer-protected gold clusters: synthesis methods, core size, and thickness of monolayer. Macromolecules 2003; 36: 4526-4533.
69. Baalousha M, Ju-Nam Y, Cole PA, Hriljac JA, Jones IP, Tyler CR, Stone V, Fernandes TF, Jepson MA, Lead JR. Characterization of cerium oxide nanoparticles-part 2: nonsize measurements. Environ Toxicol Chem 2012; 31(5): 994-1003.
70. Sanguiñedo P, Fratila RM, Estevez MB. Martínez de la Fuente J, Grazú V, Alborés S. Extracellular biosynthesis of silver nanoparticles using fungi and their antibacterial activity. Nano Biomed Eng 2018; 10(2): 165-173.
71. Heikal YM, Şutan NA, Rizwan M, Elsayed A. Green synthesized silver nanoparticles induced cytogenotoxic and genotoxic changes in *Allium cepa* L. varies with nanoparticles doses and duration of exposure. Chemosphere 2020; 243: 125430.
72. Mukherjee S, Chowdhury D, Kotcherlakota R, Patra SBV, Bhadra MP, Sreedhar B, Patra CR. Potential theranostics application of bio-synthesized silver nanoparticles (4-in-1 system). Theranostics 2014; 4(3): 316-335.
73. Feng QL, Wu J, Chen GQ, Cui FZ, Kim TN, Kim JO. A mechanistic study of the antibacterial effect of silver ions on *Escherichia coli* and *Staphylococcus aureus*. J Biomed Mater Res 2000; 52: 662-668.
74. Cho NK, Seo DS, Lee JK. Preparation and stabilization of silver colloids protected by surfactant. Materials Forum 2005; 29: 394-396.

75. Zhang M, Zhang K, Gusseme BD, Verstraete W, Field R. The antibacterial and anti-biofouling performance of biogenic silver nanoparticles by *Lactobacillus fermentum*. Biofouling 2014; 30: 347-357.
76. Guilger-Casagrande M, Germano-Costa T, Pasquoto-Stigliani T, Fraceto LF, de Lima R. Biosynthesis of silver nanoparticles employing *Trichoderma harzianum* with enzymatic stimulation for the control of *Sclerotinia sclerotiorum*. Sci Rep 2019; 9: 14351.
77. Raut RW, Mendhulkar VD, Kashid SB. Photosensitized synthesis of silver nanoparticles using *Withania Somnifera* leaf powder and silver nitrate. J Photochem Photobiol B 2014; 132: 45-55.
78. Raji V, Chakraborty M, Parikh PA. Synthesis of starch-stabilized silver nanoparticles and their antimicrobial activity. Part Sci Technol 2012; 30(6): 565-77.
79. Prozorova GF, Pozdnyakov AS, Kuznetsova NP, Korzhova SA, Emel'yanov AI, Ermakova TG, Fadeeva TV, Sosedova LM. Green synthesis of water-soluble nontoxic polymeric nanocomposites containing silver nanoparticles. Int J Nanomedicine. 2014; 9(16): 1883-1889.
80. Cakić M, Glišić S, Nikolić G, Nikolić GM, Cakić K, Cvetinov M. Synthesis, characterization and antimicrobial activity of dextran sulphate stabilized silver nanoparticles. J Mol Struct. 2016; 1110: 156-161.
81. Anandan M, Poorani G, Boomi P, Varunkumar K, Anand K, Chuturgoon AA, Gurumallesh Prabu H. Green synthesis of anisotropic silver nanoparticles from the aqueous leaf extract of *Dodonaea viscosa* with their antibacterial and anticancer activities. Process Biochem 2019; 80: 80-88.
82. Graves JrJG, Tajkarimi M, Cunningham Q, Campbell A, Nonga H, Harrison SH, Barrick JE. Rapid Evolution of Silver Nanoparticle Resistance in *Escherichia coli*. Front Genet 2015; 6: 42.
83. Panacek A, Kvitek L, Smékalová M, Večeřová M, Kolář M, Röderová M, Dycka F, Šebela M, Prucek R, Tomanec O, Zboril R. Bacterial resistance to silver nanoparticles and how to overcome it. Nat Nanotechnol 2018; 13(1): 65-71.
84. Kalishwaralal K, BarathManiKanth S, Pandian SR, Deepak V, Gurunathan S. Silver nanoparticles impede the biofilm formation by *Pseudomonas aeruginosa* and *Staphylococcus epidermidis*. Colloids Surf B Biointerfaces 2010; 79: 340-344.
85. Mohanty S, Mishra S, Jena P, Jacob B, Sarkar B, Sonawane A. An investigation on the antibacterial, cytotoxic, and antibiofilm efficacy of starch-stabilized silver nanoparticles. Nanomedicine 2012; 8: 916-924.
86. Habash MB, Park AJ, Vis EC, Harris RJ, Khursigara CM. Synergy of silver nanoparticles and aztreonam against *Pseudomonas aeruginosa* PAO1 biofilms. Antimicrob Agents Chemother 2014; 58: 5818-5830.
87. Singh P, Pandit S, Beshay M, Mokkapati VRSS, Garnaes J, Olsson ME, Sultan A, Mackevica A, Mateiu RV, Lütken H, Daugaard AE, Baun A, Mijakovic I. Anti-biofilm effects of gold and silver nanoparticles synthesized by the *Rhodiola rosea rhizome* extracts artificial cells. Artif Cells Nanomed Biotechnol 2018; 46: 886-899.
88. Mao BH, Chen ZY, Wang YJ, Yan SJ. Silver nanoparticles have lethal and sublethal adverse effects on development and longevity by inducing ROS-mediated stress responses. Sci Rep 2018; 8: 2445
89. Avalos A, Haza AI, Drosopoulou E, Mavragani-Tsipidou P, Morales P. *In vivo* genotoxicity assessment of silver nanoparticles of different sizes by the somatic mutation and recombination test (SMART) on Drosophila. Food Chem Toxicol 2015; 85: 114-119.
90. Faedmaleki F, Shirazi FH, Salarian AA, Ashtiani HA, Rastegar, H. Toxicity effect of silver nanoparticles on mice liver primary cell culture and HepG2 cell line. Iran J Pharm Res 2014; 13(1): 235-242.
91. Kim YS, Kim JS, Cho HS, Rha DS, Kim JM, Park JD, Choi BS, Lim R, Chang HK, Chung YH, Kwon IH, Jeong J, Han BS, Yu IJ. Twenty-eight day oral toxicity, genotoxicity, and gender-related issue distribution of silver nanoparticles in Sprague-Dawley rats. Inhal Toxicol 2008; 20: 575-583.
92. Murphy M, Ting K, Zhang, X, Soo C, Zheng Z. Current development of silver nanoparticle preparation, investigation, and application in the field of medicine. J Nanomater 2015; 696918.
93. Kevin WH, Kwok WD, Stella MM, Chilkoti JLA, Wiesner MR. Melissa Chernick, and David E. Hinton. Silver nanoparticle toxicity is related to coating materials and disruption of sodium concentration regulation. Nanotoxicology 2016; 10(9): 1-46.
94. Mukherjee P, Roy M, Mandal BP, Dey GK, Mukherjee PK, Ghatak J, Tyagi AK, Kale SP. Green synthesis of highly stabilized nanocrystalline silver particles by a non-pathogenic and agriculturally important fungus *T. asperellum*. Nanotechnology 2008; 19: 075103.
95. Monda S, Roy N, Laskar RA, Basu ISS, Mandal D, Begum NA. Biogenic synthesis of Ag, Au and bimetallic Au/Ag alloy nanoparticles using aqueous extract of mahogany (*Swietenia mahogani* JACQ.) leaves. Colloid Surf B 2011; 82: 497-504.
96. Greulich C, Diendorf J, Simon T, Eggeler G, Epple M, Köller M. Uptake and intracellular distribution of silver nanoparticles in human mesenchymal stem cells. Acta Biomater 2011; 7: 347-354.
97. Gil PR, Nazarenus M, Ashraf S, Parak WJ. pH-sensitive capsules as intracellular optical reporters for monitoring lysosomal pH changes upon stimulation. Small. 2012; 8: 943-948.
98. Zhang C, Jiang SZ, Huo YY, Liu AH, Xu SC, Liu XY, Sun ZC, Xu YY, Li Z, Man BY. 2015; SERS detection of R6G based on a novel graphene oxide/silver nanoparticles/silicon pyramid arrays structure. Opt Express, 2015; 23(19): 24811-24821.
99. Yu L, Zhou W, Li Y, Zhou Q, Xu H, Gao B, Wang Z. Antibacterial thin-film nanocomposite membranes incorporated with graphene oxide quantum dot-mediated silver

nanoparticles for reverse osmosis application. ACS Sustain Chem Eng 2019; 7(9): 8724-8734.